

Lithium evolution in the Galactic thin disc from Main-Sequence and early Red-Giant-Branch stars

C. T. Nguyen^{1,2}, G. Cescutti^{1,2}, F. Matteucci^{1,2,3}, F. Rizzuti^{4,2,5}, A. Mucciarelli^{6,7}, D. Romano⁶, L. Magrini⁸, A. J. Korn⁹, A. Bressan¹⁰, and L. Girardi¹¹

¹ University of Trieste, Piazzale Europa, 1, Trieste, Italy,
e-mail: chi.nguyen@inaf.it

² INAF Osservatorio Astronomico di Trieste, Via Giambattista Tiepolo, 11, Trieste, Italy

³ Institute for Fundamental Physics of the Universe, via Beirut, 2, 34151 Trieste, Italy

⁴ Heidelberger Institut für Theoretische Studien, Schloss-Wolfsbrunnenweg 35, D-69118 Heidelberg, Germany

⁵ INFN, Sezione di Trieste, via Valerio 2, I-34134 Trieste, Italy

⁶ INAF, Osservatorio di Astrofisica e Scienza dello Spazio, Via Gobetti 93/3, 40129 Bologna, Italy

⁷ Dipartimento di Fisica e Astronomia, Università degli Studi di Bologna, Via Gobetti 93/2, 40129 Bologna, Italy

⁸ INAF, Osservatorio Astrofisico di Arcetri, Largo E. Fermi 5, 50125 Firenze, Italy

⁹ Division of Astronomy and Space Physics, Department of Physics and Astronomy, Uppsala University, Box 516, SE-75120 Uppsala, Sweden

¹⁰ SISSA, Via Bonomea 265, I-34136 Trieste, Italy

¹¹ INAF - Osservatorio Astronomico di Padova, Vicolo dell'Osservatorio 5, Padova, Italy

ABSTRACT

The role of novae as producers of galactic lithium has been suggested since the 1970s, and it has been reconsidered recently with the detection of ^7Be in their outbursts. At the same time, stellar models are moving forward to comprehend the discrepancy between the primordial lithium abundance predicted by the standard Big Bang Nucleosynthesis theory and the measured value of old dwarf stars. In this work, we follow the evolution of ^7Li in the galactic thin disc starting from a primordial value of $A(\text{Li})=2.69$ dex and applying ^7Li depletion corrections of the stellar model with overshooting to our chemical evolution models. We use the upper envelope of the observational data to constrain the models. In addition to the dwarf main sequence (MS) stars, our analysis includes, for the first time, the early red-giant-branch (RGB) stars. Besides the renowned Spite plateau of the MS stars at low metallicities, we also confirm the existence of a second $A(\text{Li})$ plateau of the early RGB stars, which can be explained by our model with the corrections from stellar models. Our best-fit model is obtained with an effective averaged ^7Li yield $^{Li}Y_{\text{Nova}} = 2.34 \times 10^{-5} M_{\odot}$ during the whole lifetime of a nova. This reinforces the possibility that novae are the main galactic ^7Li source, together with the stellar models' ability to comprehend the “cosmological lithium problem” in this context.

Key words. Stars: abundances - Nuclear reactions, nucleosynthesis, abundances - (Stars:) novae, cataclysmic variables - Galaxy: abundances - Galaxy: evolution

1. Introduction

Tracing galactic ^7Li provides abundant information of the Milky Way evolution (for example, [Matteucci et al. 1995](#); [Travaglio et al. 2001](#); [Prantzos 2012](#), and references therein). Most of the models included novae as primary lithium factory ([D’Antona & Matteucci 1991](#); [Romano et al. 1999](#)), but for a long time there were no observational evidences supporting ^7Li production in nova outbursts.

Since the discovery of [Tajitsu et al. \(2015\)](#) where ^7Be was detected in the classical Nova Delphini 2013, the classical nova explosions were confirmed to be the main source of the galactic ^7Li production among other possible sources such as red giant or asymptotic giant branch (AGB) stars. Briefly after that, the discovery of [Izzo et al. \(2015\)](#) where the detection of the ^7Li I at $\lambda = 6708 \text{ \AA}$ line in the spectra of Nova Centauri 2013 (V1369Cen) was reported. This was further supported by the detection of the isotope ^7Be in many other novae ([Molaro et al. 2016](#); [Tajitsu et al. 2016](#); [Izzo et al. 2018](#); [Molaro et al. 2020b](#); [Arai et al. 2021](#); [Molaro et al. 2022, 2023](#)). Currently, a possible detection of a 478 keV emission line emitted in the ^7Be decay

into ^7Li has been reported by [Izzo et al. \(2025\)](#) for V1369Cen. This is due to the short-lived lifetime of ^7Be (~ 53 days) and its decay into ^7Li . Indeed, an amount of ejected ^7Li per nova event, $\approx 1 - 10 \times 10^{-9} M_{\odot}$, was determined in these cases. This strongly indicates that the main source of ^7Li production in the Milky Way is from nova systems.

During the last decade, observational surveys have provided a huge amount of data for lithium abundance, from galactic discs to the bulge, from star clusters to halo field stars, from the main-sequence (MS) to the advanced red-giant and asymptotic-giant branch evolutions. For example, the Gaia-ESO survey ([Fu et al. 2018](#); [Randich et al. 2020](#); [Magrini et al. 2021](#); [Romano et al. 2021](#)), the Galactic Archaeology with HERMES survey (GALAH, [De Silva et al. 2015](#); [Wang et al. 2024](#)), the Large Sky Area Multi-Object Fiber Spectroscopic Telescope survey (LAMOST, [Gao et al. 2019](#); [Ding et al. 2024](#)), and the upcoming 4MOST Milky way Disc And BuLgE High-Resolution survey (4MIDABLE-HR, [Bensby et al. 2019](#)).

The surveys are a great source of observational data for chemical evolution models to study precisely the properties of

the galactic lithium evolution. In particular, various models recently claim the importance of novae for the enrichment of ${}^7\text{Li}$ in the solar neighbourhood, for example, [Cescutti & Molaro \(2019\)](#), [Romano et al. \(2021\)](#), [Gao et al. \(2024\)](#), and [Borisov et al. \(2024\)](#). These works agreed on the fact that novae are the main production source of the galactic ${}^7\text{Li}$. However, the precise amount of lithium yield per nova event differs between different works. In particular, [Cescutti & Molaro \(2019\)](#) claimed an amount of $1.8 \times 10^{-9} M_{\odot}$ to be the best-fit value (assuming about 10^4 explosion events occur during the whole lifetime of novae), while [Borisov et al. \(2024\)](#) claimed a ~ 3 times larger value, $5 \times 10^{-9} M_{\odot}$ with their one-zone model (with assuming an average mass of the ejecta of $5 \times 10^{-5} M_{\odot}$ in a novae lifetime).

On the other side, the observed metal-poor dwarf stars ($[\text{Fe}/\text{H}] \leq -1$) indicate an A(Li) plateau commonly known as the Spite plateau (A(Li) ≈ 2.2 dex, [Spite & Spite 1982a,b](#); [Bonifacio 2002](#); [Charbonnel & Primas 2005](#); [Korn et al. 2007](#)). This measured value is about ~ 3 times smaller than the predicted primordial value which is obtained from the Big Bang Nucleosynthesis studies (A(Li) ≈ 2.7 dex, [Coc et al. 2014](#); [Cyburt et al. 2016](#); [Singh et al. 2019](#); [Iliadis & Coc 2020](#); [Pitrou et al. 2021](#); [Singh et al. 2024](#)) assuming the cosmological parameters determined by Planck ([Planck Collaboration et al. 2014](#)). The origin of this discrepancy is still debated, and is usually known as the “cosmological lithium problem”. For example, [Eggenberger et al. \(2012\)](#), [Fu et al. \(2015\)](#) and [Nguyen et al. \(2025\)](#) proposed different mechanisms with ${}^7\text{Li}$ depletion during the PMS evolution, while [Richard et al. \(2005\)](#) moderated the atomic diffusion with turbulence mixing during the MS. Recently, [Nguyen et al. \(2025\)](#) provided a grid of stellar models, where the envelope overshooting efficiency parameter was modified during the PMS evolution of the stars towards comprehending this issue. Their models were calibrated with the renowned globular cluster NGC 6397. Taking advantage of this grid, we explored their models to predict the amount of ${}^7\text{Li}$ depletion from the primordial value (A(Li) = 2.69 dex), and applied it to our chemical evolution models in order to investigate the evolution of the galactic ${}^7\text{Li}$ from the metal-poor to the metal-rich regions.

Moreover, recently [Mucciarelli et al. \(2022\)](#) discovered a thin plateau among the metal-poor red-giant-branch (RGB) stars. Their sample contains 58 early RGB stars with metallicity ranges $-7 \leq [\text{Fe}/\text{H}] \leq -1.3$, and high-resolution spectra were used for the derivation of A(Li). The authors discovered a plateau (with the mean value A(Li) = 1.09 ± 0.08 dex) for these early RGB metal-poor stars that is similar to the one for MS stars (or the so-called Spite plateau [Spite & Spite \(1982a,b\)](#)). Hence, in this work, we also study the behaviour of A(Li) at this early RGB evolution to investigate this discovered plateau and the role of nova production to ${}^7\text{Li}$ at this evolutionary stage. For this purpose, we selected two subsamples of dwarf-MS and early-RGB stars from the recent catalogues of GALAH DR4 ([Wang et al. 2024](#)), and Gaia-ESO ([Magrini et al. 2021](#); [Romano et al. 2021](#)), complemented with the sample of F and G dwarf-MS stars from [Bensby & Lind \(2018\)](#).

The paper is organised into six sections. In Sect. 2, we describe the methodology to select our data samples from the big surveys GALAH and Gaia-ESO. Section 3 shows the predictions from the stellar models regarding the depletion of A(Li) from the primordial value. In Sect. 4, we describe the chemical evolution model that is used for this work. We present the obtained results in Sect. 5 and draw our conclusions in Sect. 6.

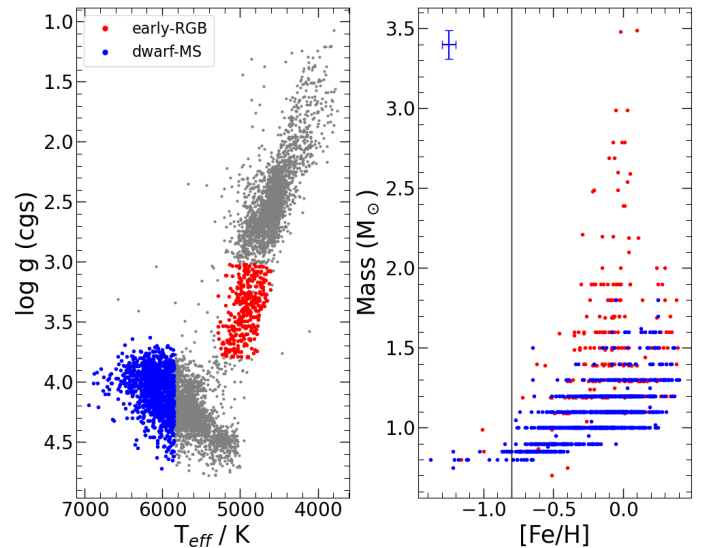


Fig. 1. Left panel: the sample of 7347 field stars from [Magrini et al. \(2021\)](#), with our selected subsamples highlighted in red and blue. Right panel: the mass distribution with metallicity ($[\text{Fe}/\text{H}]$) of stars in our selected samples. The blue error bar indicates the mean uncertainty value of our selected dwarf-MS sample. The black vertical line marks for $[\text{Fe}/\text{H}] = -0.8$ dex.

2. Sample selection

The catalogue of [Magrini et al. \(2021\)](#) presents high-quality data from the Gaia-ESO iDR6 survey. It contains 7347 field stars with metallicity in the range $-1 \leq [\text{Fe}/\text{H}] \leq 0.5$ dex. The ${}^7\text{Li}$ abundances are derived with the one-dimensional (1D) local thermodynamic equilibrium (LTE) assumption ([Franciosini et al. 2022](#)). We selected two subsamples of dwarf-MS stars ($\log g > 3.6$ and $T_{\text{eff}} \geq 5850$ K) and early RGB stars ($3.1 \leq \log g \leq 3.8$ and $4600 \leq T_{\text{eff}}/\text{K} \leq 5300$) for our analysis in this work. The choice of $\log g$ and T_{eff} is made to avoid the stars that are going through the ${}^7\text{Li}$ depletion due to convective-driven and thermohaline mixing. The selected samples are shown in the left panel of Fig. 1. Note that we already excluded Li-rich stars in our samples in Fig. 1, based on the definition found in [Magrini et al. \(2021\)](#), namely, $A(\text{Li}) \geq 2.0$ dex, $3800 \leq T_{\text{eff}}/\text{K} \leq 5000$, $\log g \leq 3.5$ and the gravity index $\gamma \geq 0.98$. Furthermore, the mass of each star is reported in the Gaia-ESO catalogue (see [Magrini et al. 2021](#)). We show in the right panel of Fig. 1 the mass distribution of stars in the two subsamples. In particular, the metal-poor stars ($[\text{Fe}/\text{H}] \leq -0.8$) are, in fact, low-mass stars with masses about $\sim 0.8 M_{\odot}$. Within the uncertainty, they seem to always be below $1 M_{\odot}$. This encourages us to explore the correction from available stellar models on the variation of lithium abundances, which will be described in the next section. We also adopted the catalogue from [Romano et al. \(2021\)](#) that includes carefully selected 26 open clusters, and 3210 field stars from the Gaia-ESO iDR6 survey. This sample also contains important information such as the stellar ages and galactocentric distances. We applied the same selection method as the previous sample, meaning $\log g > 3.6$ and $T_{\text{eff}}/\text{K} \geq 5850$.

The GALAH survey also provides us with another opportunity to study the chemical history of the Milky Way using high-resolution spectroscopy. Lithium is one of the main focuses of the survey, [Wang et al. \(2024\)](#) provided 3D non-LTE (3D-NLTE) ${}^7\text{Li}$ abundance for 581149 field stars released in GALAH DR3 ([Buder et al. 2021](#)). In this work, we adopted the catalogue with three additional conditions for our selected samples. They are

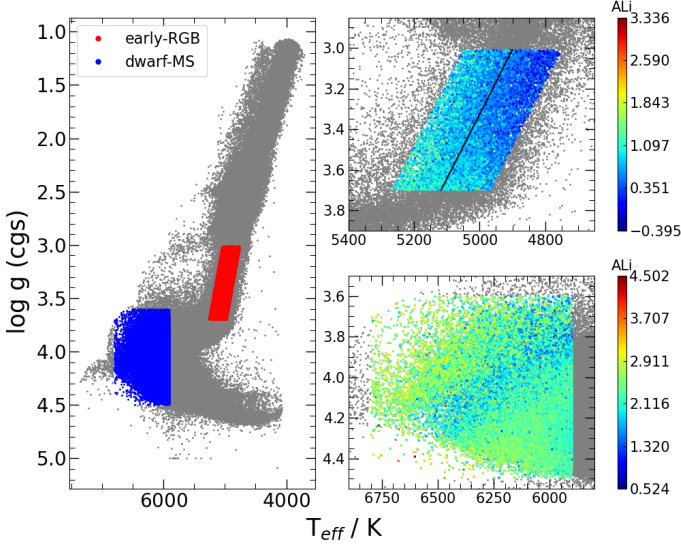


Fig. 2. Left panel: the complete sample of lithium detection adopted from the GALAH DR4 catalogue (grey dots). Our two selected samples are highlighted in blue and red. Top-right panel: zoom in on our selected early RGB stars sample, with the colour bar indicating $A(\text{Li})$. Bottom-right panel: our selected dwarf-MS stars sample. See the text for details of the selections.

with flags: i) `flag_ALi` = 0, which means only 228 613 field stars with actual lithium detection are used; ii) `flag_fe_h` = 0 and iii) `flag_sp` = 0, which mean no problem noted from the observational analysis. The full sample is presented on the left panel of Fig. 2. Our subsamples for the dwarf-MS and the early RGB stars are highlighted in blue and red colours, respectively.

First, for the dwarf-MS sample, we made a selection of stars with $3.6 < \log g < 4.5$ and $5850 \leq T_{\text{eff}}/\text{K} \leq 6800$. These choices of $\log g$ and T_{eff} are also to avoid the contamination from stars that are undergoing the convection-driven ${}^7\text{Li}$ depletion. We obtained about 97 193 stars for this subsample, which are shown in the bottom-right panel of Fig. 2.

Then, for our early RGB stars, to avoid the distraction from the red clump stars, we selected stars with $3.0 < \log g < 3.7$. After that, for a narrow region within $4500 < T_{\text{eff}} < 5500$ K, we search for the synthetic line which mimics the RGB evolution in this region by using the simple `polyfit` python function, which is plotted by the black line on the top-right panel of Fig. 2. After that, we selected the stars within the range of $T_{\text{eff}}^{\text{synthetic}} \pm 150$ K for our early RGB sample. As a result, we obtained about 15 316 RGB stars for our sample.

Furthermore, we adopted the catalogue from Bensby & Lind (2018), which contains in total 714 F, G-dwarf, turn-off, and subgiant stars. However, we selected only 275 stars with the actual detected ${}^7\text{Li}$ abundances and $T_{\text{eff}} \geq 5850$ K for our sample. The ${}^7\text{Li}$ abundances in this catalogue were derived with 1D-LTE analysis of high-resolution spectra.

3. Predictions from stellar models

Nguyen et al. (2025) introduces stellar models with different values of envelope overshooting efficiency parameter between the pre-main-sequence and the post-main-sequence evolutions, to reproduce the ${}^7\text{Li}$ plateau at the MS and the RGB bump location of the GC NGC 6397, by using the PARSEC code (see also Bressan et al. 2012; Nguyen et al. 2022, for more information). In particular, a value of $\Lambda_e = 0.6H_p$ is applied to the post-MS

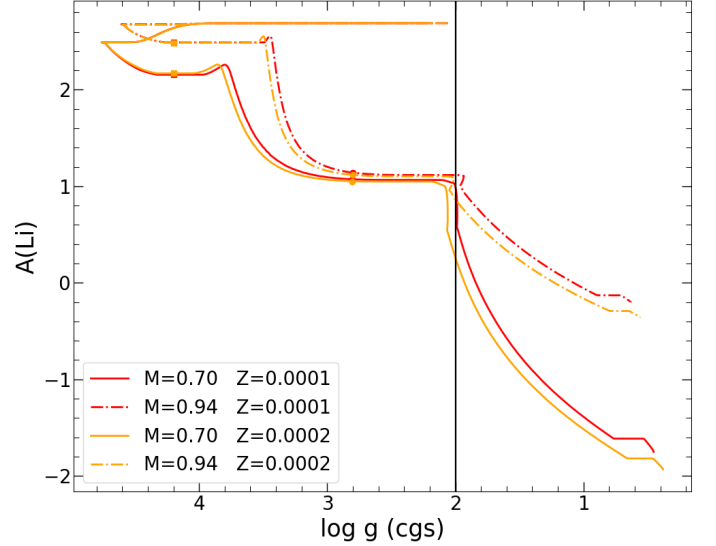


Fig. 3. The variation of surface ${}^7\text{Li}$ abundance with $\log g$ of four selected stellar models. The square symbol marks the location where $\log g \sim 4.1$ at the MS, while the circle symbol is where $\log g \sim 2.8$ at the early RGB. The black line indicates $\log g \sim 2$ around the RGB bump.

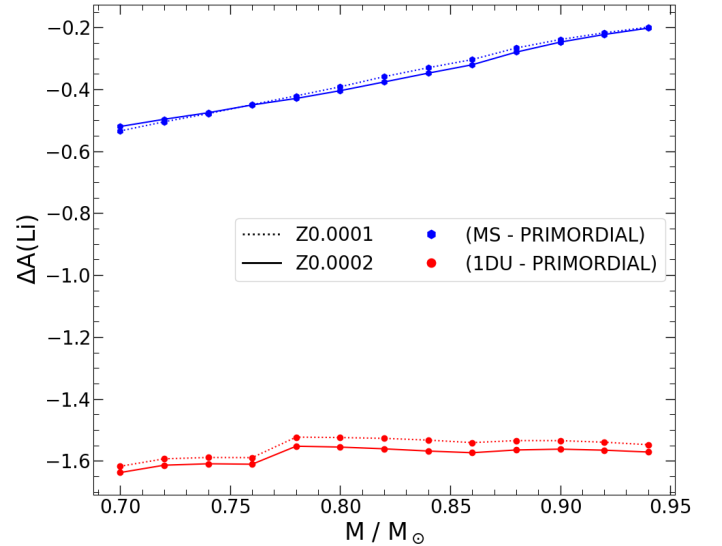


Fig. 4. Depletion of lithium abundance up to the MS (blue) and the 1DU at the early RGB phase (red). The models are taken from Nguyen et al. (2025) with the depletion during the PMS phase due to the envelope overshooting taken into account.

evolution to calibrate the RGB bump, and a smaller value of $\Lambda_e^p = 0.05 - 0.6H_p$ (that is dependent on the initial masses) is applied to the early PMS evolution, where H_p is the pressure scale height. As a result, a depletion from the primordial value ($A(\text{Li}) = 2.69$ dex, Coc et al. 2014, as the initial value applied to the stellar models) to the measured value in dwarf, turn off and subgiant stars of NGC 6397 ($A(\text{Li}) \approx 2.22$ dex, Lind et al. 2009)) is obtained.

As mentioned above, the observed metal-poor stars ($[\text{Fe}/\text{H}] \leq -0.8$) show a mass range of about $0.8 - 1.0M_{\odot}$. Nguyen et al. (2025) provides models with $M \sim 0.7 - 0.94M_{\odot}$ for two metallicity set $Z = 0.0001, 0.0002$ ($[\text{Fe}/\text{H}] \approx -2.4, -2.1$). Fig. 3 shows the variation of $A(\text{Li})$ with $\log g$ of four selected models at the boundary limit of the sets. All models evolve from the PMS (begins at $\log g \sim 2.2$, $A(\text{Li}) = 2.69$) towards higher

$\log g$ and make the turning point at the zero-age-MS (ZAMS). The variation of $A(\text{Li})$ during this phase shows a clear depletion due to the efficiency of the envelope overshooting, which mainly depends on mass. After that, atomic diffusion causes further depletion of $A(\text{Li})$ from the ZAMS until the end of the MS, where mixing partially restores it. The squared symbols mark the location where diffusion shows its maximum efficiency. Subsequently, the convective envelope penetrates toward inner layers, which leads to the dilution of ${}^7\text{Li}$ in the envelope. This dilution process leads to a significant depletion during this evolutionary phase until it reaches a constant value when the 1DU is completed during the RGB phase (dotted symbols). The thermohaline mixing becomes active and depletes even more $A(\text{Li})$ at the more advanced evolution above the RGB bump (see also Charbonnel & Zahn 2007, and references therein).

Figure 4 shows the difference of lithium abundances from the initial value ($A(\text{Li}) = 2.69$ dex) to the MS ($\log g \sim 4.1$) and the RGB (before the so-called RGB bump) when the first dredge-up is already completed ($\log g \sim 2.8$). The theoretical prediction indicates an overall depletion from the initial value throughout the entire evolution of the stars. Firstly, within the presented mass and metallicity ranges, a depletion of $\sim 0.2 - 0.5$ dex can be seen from the primordial value at the MS phase. Especially in the mass range $\leq 0.8M_{\odot}$ that shows a depletion of $\sim 0.4 - 0.5$ dex, which is the typical value that is needed to reproduce the Spite plateau ($A(\text{Li}) \approx 2.2$ dex, Spite & Spite 1982a,b).

Secondly, within the typical uncertainty (≈ 0.1 dex), the depletion after the 1DU from the initial value shows an approximately constant value, that is, $\Delta A(\text{Li}) \approx 1.6$ dex for all shown models. This prediction indicates the existence of a second plateau that is located at the early RGB evolution, where the stars do not suffer yet from the effect of thermohaline mixing, which confirms the observational results obtained by Mucciarelli et al. (2022). This aspect will be discussed in the results section below.

4. Chemical evolution model

4.1. Model for thin disc

In order to study the lithium evolution of the thin disc of the Milky Way, we adopted the model introduced by Cescutti & Molaro (2019). We point the reader to Cescutti & Molaro (2019) for more details about the model, while we here only summarise the main ingredients for our work. In particular, the initial mass function (IMF) is adopted from Kroupa (2001), and the stellar lifetimes follow Meynet & Maeder (2002). The single degenerate scheme for the progenitors of SNe Ia is adopted from Matteucci & Greggio (1986). We assume the thin disc to be formed by slow gas infall (for details see Cescutti & Molaro (2019)).

The key ingredient of this model for lithium is the assumption that nova systems are the principal producers of ${}^7\text{Li}$, although we also consider a small contribution from cosmic rays (see Prantzos 2012). The nova rate is computed by assuming the same delay time distribution (DTD) of the SNe Ia deriving from cataclysmic variables (single degenerate scenario) as in Matteucci & Greggio (1986), but with an additional time delay to allow for the cooling of the white dwarfs.

In Cescutti & Molaro (2019), it was assumed that only binary systems formed by stars in the mass range $M = 0.8 - 8M_{\odot}$ can develop nova systems. The probability of forming a binary system of a certain mass is weighted on the IMF. The configurations

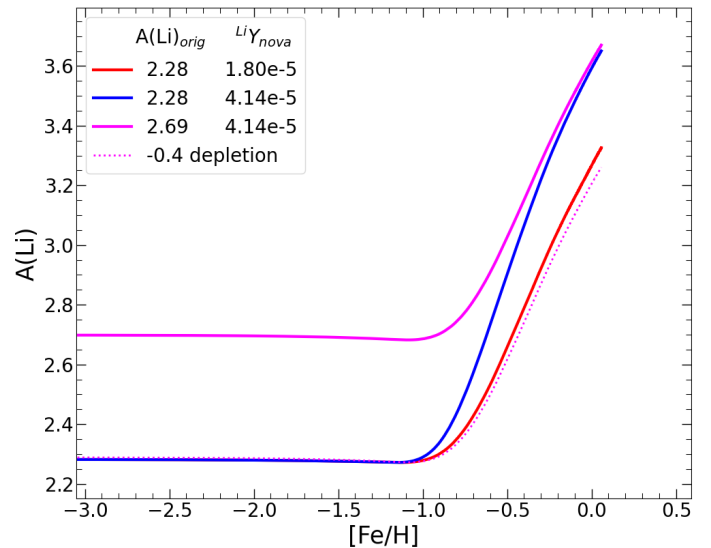


Fig. 5. Chemical evolution models of lithium with different adopted values of original ${}^7\text{Li}$ abundance and novae yields, as listed in the figure legend. An illustration model with -0.4 dex depletion from the primordial $A(\text{Li}) = 2.69$ model (magenta line) is plotted as the dotted line.

of primary and secondary stars are defined by

$$f(\mu) = 2^{1+\gamma}(1+\gamma)\mu^{\gamma}. \quad (1)$$

Where $f(\mu)$ is the distribution function for the mass fraction of the secondary star, $\mu = M_2/M_B$, where M_2 is the mass of the secondary star and M_B is the mass of the binary system. The exponent coefficient $\gamma = 2$ is adopted from Greggio & Renzini (1983).

The fraction of binary systems that develop a nova thus becomes a crucial parameter in the model. This parameter is defined by N_{lithium} . In this work, we keep using the proposed fraction by Cescutti & Molaro (2019), that is $N_{\text{lithium}} = 0.03$, which corresponds to a Galactic rate of nova bursts at present of $\sim 20 - 30 \text{ yr}^{-1}$ (see Shafter 1997; Della Valle & Izzo 2020).

The time when ${}^7\text{Li}$ production takes place is defined as the time at which the primary star evolves into a white dwarf plus a so-called delay time, τ_{nova} . In particular, τ_{nova} is the time needed for a white dwarf to ignite the first nova outburst, which can occur only after the cooling of the white dwarf. Cescutti & Molaro (2019) found $\tau_{\text{nova}} = 1 \text{ Gyr}$ to be the best-constrained value, and in agreement with the previous works (e.g. Romano et al. 2001; Izzo et al. 2015), thus we adopted this value in this work.

The total ${}^7\text{Li}$ produced by a nova during its lifetime is defined as ${}^{Li}Y_{\text{Nova}}$. The assumption that all novae produce the same amount of ${}^7\text{Li}$ in all events is also adopted in this work. A value of ${}^{Li}Y_{\text{Nova}} = 1.8 \times 10^{-5}M_{\odot}$, with a typical number of 10^4 outbursts events during the entire lifetime of novae (Ford 1978), is also suggested in the model of Cescutti & Molaro (2019), where they assumed the measured ${}^7\text{Li}$ abundance from the dwarf halo stars, $A(\text{Li}) = 2.28$ dex, as the initial gas composition. For many years, this abundance has been assumed to be the primordial one until the Wilkinson Microwave Anisotropy Probe (WMAP) and Planck satellites suggested that the primordial ${}^7\text{Li}$ abundance is three times higher ($A(\text{Li}) = 2.69$ dex, e.g. Cyburt et al. 2003; Coc et al. 2004).

The predicted evolution of $A(\text{Li})$ with metallicity $[\text{Fe}/\text{H}]$ is shown in Fig. 5. It is clear that since ${}^7\text{Li}$ is mainly produced by novae on long timescales, the abundance of ${}^7\text{Li}$ for $[\text{Fe}/\text{H}] < -1$ is the initial one, which could be the primordial value. On the

other hand, the contribution from novae explosions is dominant in the more metal-rich region. It is worth noting that the chemical evolution model predicts the evolution of ^7Li in the interstellar medium, and when we compare our results with the ^7Li abundance measured in the atmospheres of stars, we assume that it has not been depleted, and therefore, we aim to reproduce the upper envelope of the data. However, if the ^7Li has indeed been depleted, this comparison should take the depletion into account. In the figure, we show models starting from an initial ^7Li abundance as observed in halo stars (2.28 dex) and models starting with the primordial ^7Li suggested by Planck (2.69 dex). The comparison between models with the same $^{Li}Y_{\text{Nova}}$ but different original $A(\text{Li})$ values shows a clear trend of convergence towards higher metallicity. This means that the production of novae overcomes the difference in original abundances as the galaxy evolves. However, if a model with the primordial lithium as its original composition, and depletion due to the evolution of stars is assumed (dotted line), a higher nova ^7Li yield is required to reproduce the prediction of the model with a lower original $A(\text{Li})$. This was suggested in Cescutti & Molaro (2019), where $^{Li}Y_{\text{Nova}} = 4.14 \times 10^{-5} M_{\odot}$ if the primordial $A(\text{Li})$ is used as the original abundance and a fixed amount of depletion is assumed.

In this work, we explore the model computed with the primordial lithium abundance, $A(\text{Li})=2.69$ dex, and apply the depletion corrections from stellar models of Nguyen et al. (2025). In other words, the evolution of ^7Li is now expressed as follows,

$$A(\text{Li}) = A(\text{Li})_{\text{CEM}} + \Delta A(\text{Li})_{\text{SM}}, \quad (2)$$

where $A(\text{Li})_{\text{CEM}}$ is obtained from the chemical evolution model, with the variables are original ^7Li abundance and the novae ^7Li yield that applied to the model. $\Delta A(\text{Li})_{\text{SM}}$ is the predicted correction from stellar models, which depends on mass and metallicity, as will be shown below.

4.2. Correction from stellar models

As described in Sect. 3, the grid of stellar models covers the mass ranges from $0.70 - 0.94 M_{\odot}$ and metallicity $-2.4 \leq [\text{Fe}/\text{H}] \leq -2.1$ are taken from Nguyen et al. (2025). Within the models, a depletion $\Delta A(\text{Li}) \approx 0.2 - 0.5$ dex from the primordial value ($A(\text{Li}) = 2.69$ dex) at the MS phase mainly depends on the stellar masses. On the other hand, a depletion of around 1.52-1.63 dex is predicted for stars at the early RGB phase, which also depends on mass and metallicity. Therefore, to determine the amount of depletion at a given point of the lithium evolution (in the plane of $A(\text{Li})$ versus $[\text{Fe}/\text{H}]$), the metallicity and mass at this point are needed.

In Fig. 6, we show the mass distribution of the selected dwarf-MS and early RGB stars from the GALAH catalogue (top- and bottom-panels correspondingly). The figure indicates the lowest mass presented in the samples is $\sim 0.7 M_{\odot}$, which is covered by the stellar grid of Nguyen et al. (2025). It also clearly indicates different trends between stars below and above $[\text{Fe}/\text{H}] \sim -0.75$, especially in the case of dwarf-MS stars. However, the grid that is used in this work is limited to $0.94 M_{\odot}$. Therefore, we adopt the depletion predicted by this $0.94 M_{\odot}$ model for higher masses. We divide the samples into three regions: below $[\text{Fe}/\text{H}] \leq -0.85$; between $-0.85 < [\text{Fe}/\text{H}] < -0.65$; and above $[\text{Fe}/\text{H}] \geq -0.65$. We used the polyfit function to obtain the empirical relation of mass and metallicity for the stars within the first two regions, which are plotted in red and orange in Fig. 6.

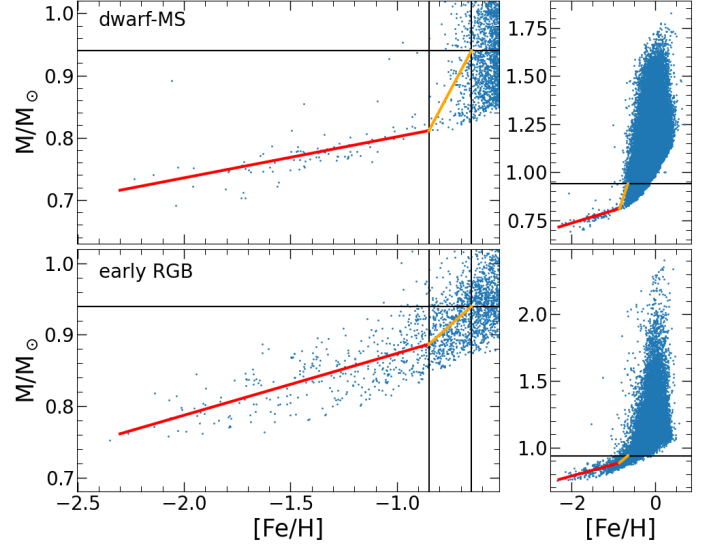


Fig. 6. Mass distribution with metallicity in two samples of dwarf-MS (top panel) and early RGB (bottom panel) selected from the GALAH catalogue. The left panels zoom in on the low-mass and metal-poor area. The right panels show the whole sample. The empirical relations at two regions of $[\text{Fe}/\text{H}]$ are shown in red and orange solid lines. The black horizontal line indicates the mass limit $0.94 M_{\odot}$, while the vertical lines indicate the metallicity $[\text{Fe}/\text{H}] = -0.85$ and -0.65 .

Table 1. Adopted values in each presented model.

Name	Description		
	$A(\text{Li})_{\text{orig}}$	$^{Li}Y_{\text{Nova}}$	depletion
model A	2.69	$2.34 \times 10^{-5} M_{\odot}$	without
model B	2.69	$2.34 \times 10^{-5} M_{\odot}$	with
model C	2.28	$1.8 \times 10^{-5} M_{\odot}$	without

As a result, we obtained the relations,

$$M = 0.066[\text{Fe}/\text{H}] + 0.867, \text{ for } [\text{Fe}/\text{H}] \leq -0.85, \quad (3)$$

$$M = 0.643[\text{Fe}/\text{H}] + 1.358, \text{ for } [\text{Fe}/\text{H}] = [-0.85, -0.65]. \quad (4)$$

Similarly, we obtained the relations for early RGB stars as follows,

$$M = 0.086[\text{Fe}/\text{H}] + 0.960, \text{ for } [\text{Fe}/\text{H}] \leq -0.85, \quad (5)$$

$$M = 0.265[\text{Fe}/\text{H}] + 1.112, \text{ for } [\text{Fe}/\text{H}] = [-0.85, -0.65]. \quad (6)$$

The empirical relations above establish the relation between mass and metallicity. In other words, at a given metallicity $[\text{Fe}/\text{H}]$ along the evolution of lithium, we can deduce the mass and thus determine the amount of depletion that is predicted from the stellar grid. For this purpose, we applied the linear interpolation method in mass and metallicity from the stellar grid to obtain the predicted amount of depletion at a given point of the $A(\text{Li})$ evolution. In this regard, for masses below $0.7 M_{\odot}$, the predicted depletion of the $0.7 M_{\odot}$ model is adopted, and for masses above $0.94 M_{\odot}$, the predicted depletion of the $0.94 M_{\odot}$ model is adopted.

5. Results

As mentioned above, the presented models in this work adopt the primordial lithium, which is constrained by the number of baryons per photon from the WMAP satellite or the cosmological parameters determined by Planck (Komatsu et al. 2011; Coc

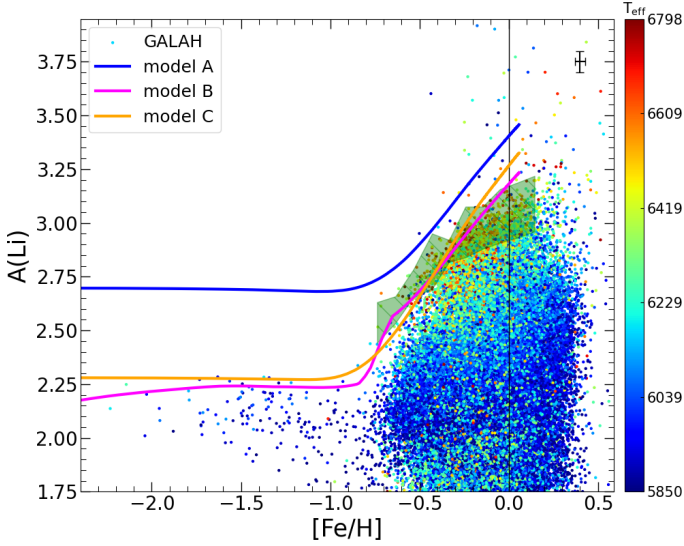


Fig. 7. Lithium abundances versus metallicity of dwarf-MS stars from the GALAH sample, colour-coded by their effective temperatures. Our models with and without stellar correction are shown in magenta and blue lines, respectively (see Table. 1). The defined upper envelope is shown by the green-shaded area. The error bars indicate the mean uncertainties of the observed data. The black vertical line marks for $[\text{Fe}/\text{H}] = 0$.

et al. 2014), that is $A(\text{Li})=2.69$ dex. The models with/without taking into account the corrections predicted from stellar models (Sect. 3) are then directly compared to the field stars at two evolutionary stages, namely, the dwarf-MS and the early-RGB evolution (below the bump) as selected from Sect. 2. Different models with varying values of original $A(\text{Li})$ and $^{Li}Y_{\text{Nova}}$ are summarised in Table. 1.

5.1. Dwarf main sequence stars

First of all, we compute models with different ^7Li yields and the primordial lithium value, $A(\text{Li}) = 2.69$ dex. The correction from stellar models is then added to the evolution of ^7Li following the description in Sect. 4.2.

Secondly, we define an upper envelope for the stars with $[\text{Fe}/\text{H}] \geq -0.8$ dex by computing the mean value of 0.1% highest $A(\text{Li})$ data points in each bin over 10 bins of 0.1 dex in $[\text{Fe}/\text{H}]$, with the minimum number of stars set to 5. The envelope is then constructed by one standard deviation from the mean values of each bin, as shown in Fig. 7. Meanwhile, the large spread of $A(\text{Li})$ in this region might have many mechanisms at work, for instance, the stellar internal rotation and angular momentum transport process (e.g. Eggenberger et al. 2022, and references therein), or the intrinsic properties of those stars (e.g. Dantas et al. 2025, and references therein). Additionally, there are stars with extremely high $A(\text{Li})$ in the region with $[\text{Fe}/\text{H}] > -0.4$ dex. As claimed in the literature, the origins of these stars remained unclear (see Koch et al. 2012; Gao et al. 2020). An investigation into these stars is beyond the scope of this paper and is worth a separate study soon.

As a result, Fig. 7 claims model B with $A(\text{Li})=2.69$, $^{Li}Y_{\text{Nova}} = 2.34 \times 10^{-5} M_{\odot}$, with the correction from the stellar model is the best-fit model. In the low metallicity region ($-2.5 < [\text{Fe}/\text{H}] < -0.8$ dex), our model reproduces very well the Spite plateau, $A(\text{Li}) = 2.15 - 2.25$ dex (with $-2.5 \leq [\text{Fe}/\text{H}] \leq -0.9$). In the higher metallicity region, our best-fit model reproduces

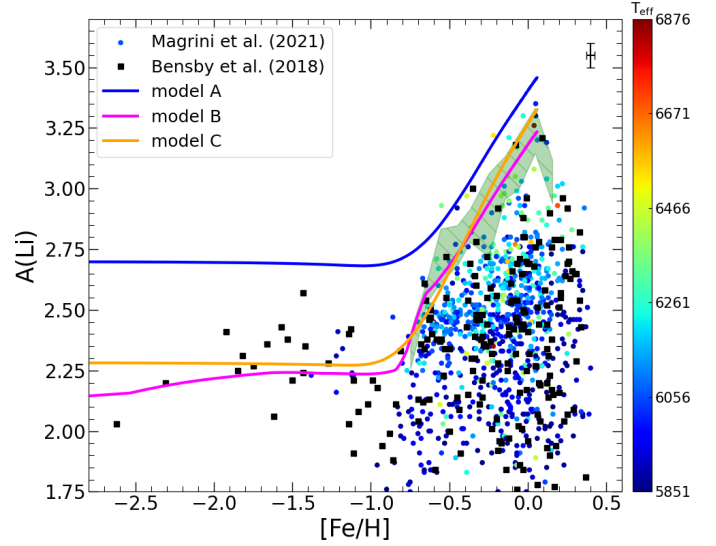


Fig. 8. Li-abundance versus metallicity of dwarf-MS field stars from the Gaia-ESO (Magrini et al. 2021) and Bensby et al. catalogues. The models shown in Fig. 7 are also adopted in this plot. The black error bars indicate the mean uncertainties of the Bensby et al. sample.

very well the defined upper envelope. At $[\text{Fe}/\text{H}] = 0$, our model shows $A(\text{Li}) = 3.16$ dex and a depletion predicted from stellar model of -0.22 dex, which is consistent with the meteoritic value $A(\text{Li}) \sim 3.33$ (Lodders et al. 2009).

The sample of dwarf-MS field stars from the Gaia-ESO catalogue is shown in Fig. 8. We also included 275 stars from Bensby & Lind (2018) with the metallicity extending to ~ -2.6 dex. The upper envelope is drawn from the sample of Gaia-ESO data (Magrini et al. 2021) for the comparison. Within the typical uncertainty of $A(\text{Li})$ that is ~ 0.1 dex, our model reproduces very well the Spite plateau region. The comparison to the defined upper envelope suggests the best-fit model is with $^{Li}Y_{\text{Nova}} = 2.34 \times 10^{-5} M_{\odot}$, which is in agreement with the GALAH data in Fig. 7.

The sample of ~ 700 field stars and the averaged ^7Li abundances of 13 open clusters in the solar vicinity (with the galactocentric distance between 7 – 9 kpc) selected from the catalogue of Romano et al. (2021) are shown in Fig. 9. On the left panel, the upper envelope of field stars of this sample shows a remarkable agreement with the other three catalogues for our best-constrained model (model B). Most clusters have $A(\text{Li})$ within the defined envelope, except for two clusters that are circled in red. However, we also note that their uncertainties are $\sigma_{A(\text{Li})} = 0.1$ and 0.13 dex for IC 4665 and ρOph , respectively. The right panel of Fig. 9 shows the abundances of ^7Li with ages (in Myr). Note that in this case, we define the upper envelope by considering 20 bins of 500 Myr starting from 1000 Myr. The black solid line indicates the time when the sun formed 4.6 Billion Years ago. The prediction of the model for the interstellar medium is of $A(\text{Li}) \sim 3.1$ dex, which is 0.2 lower than the meteoritic value ($A(\text{Li}) \sim 3.3$, Lodders et al. 2009); this may indicate that the Sun was born from a inner Galactic region, compared to stars that are present now in the solar vicinity.

However, we should clarify two points: first, the uncertainties in the stellar ages prevent us from drawing firm conclusions based on this diagram; second, we consider the yields from novae and their formation channels to be constant; however, possible metal dependencies could influence and improve the fit. We decided to reserve a more complex treatment for future work. In

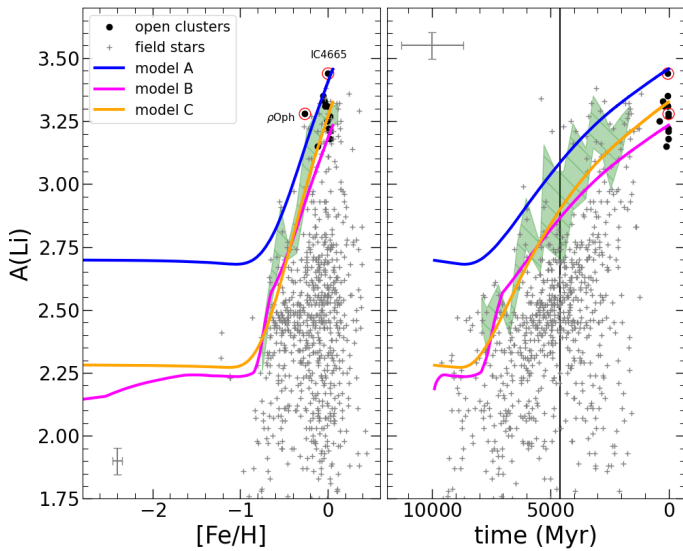


Fig. 9. Li abundances of open clusters and field stars from the Gaia-ESO catalogue (Romano et al. 2021) as a function of metallicity (left panel), and stellar age (right panel). The models shown in Fig. 7 are also adopted in this plot. The grey error bars indicate the mean uncertainties. The shaded area indicates the defined envelope computed with the field stars. The black vertical line on the right panel is for age 4.6 Gyr.

any case, the agreement between four catalogues on the $A(\text{Li})$ versus $[\text{Fe}/\text{H}]$ diagram, in return, supports our evolution model.

In addition to that, we also show in Figs. 7, 8 and 9 the model computed with the Spite plateau value ($A(\text{Li}) = 2.28$ dex) for the sake of comparison. We find agreement with Cescutti & Molaro (2019) that the model with lithium yield $^{Li}Y_{\text{Nova}} = 1.8 \times 10^{-5} M_{\odot}$ would be the best-constrained value if the original gas composition is assumed to be the one measured at the Spite plateau. On the other hand, this model will predict a lithium abundance in the presolar material quite low, not compatible with the measured one.

5.2. Early RGB stars

In Sect. 3, we found that stellar models with different masses and metallicities show a possible plateau at the RGB evolution after the 1DU and before the RGB bump. The depletion from the primordial value ($A(\text{Li}) = 2.69$ dex) is about ~ 1.6 dex at this evolutionary stage.

In Fig. 10, we explore this finding with a sample selected from the GALAH catalogue. Our selected sample was described in Sect. 2. Moreover, for the fitting purpose, we excluded the Li-rich stars by using the definition of Magrini et al. (2021). In total, we obtained a sample of 15 297 early RGB stars from the GALAH catalogue, with $-2.14 \leq [\text{Fe}/\text{H}] \leq 0.48$, $4750 \leq T_{\text{eff}}/\text{K} \leq 5270$, and $3 \leq \log g \leq 3.7$.

Indeed, the data in Fig. 10 shows a plateau feature of $A(\text{Li})$ in the low metallicity region, $[\text{Fe}/\text{H}] \leq -0.9$, with $A(\text{Li}) \sim 1.0$ – 1.2 dex at the upper limit. Meanwhile, $A(\text{Li})$ is about 1.8 – 1.9 dex at $[\text{Fe}/\text{H}] = 0$. These typical values are about 1.1 – 1.3 dex lower than the dwarf-MS stars in Figs. 7 and 8.

Our chemical evolution model with the depletion from stellar evolution correction, assuming $A(\text{Li}) = 2.69$ and $^{Li}Y_{\text{Nova}} = 2.34 \times 10^{-5} M_{\odot}$, reproduces very well the early RGB plateau as can be seen in Fig. 10. Moreover, this model also fits very well the upper envelope in the higher metallicity region.

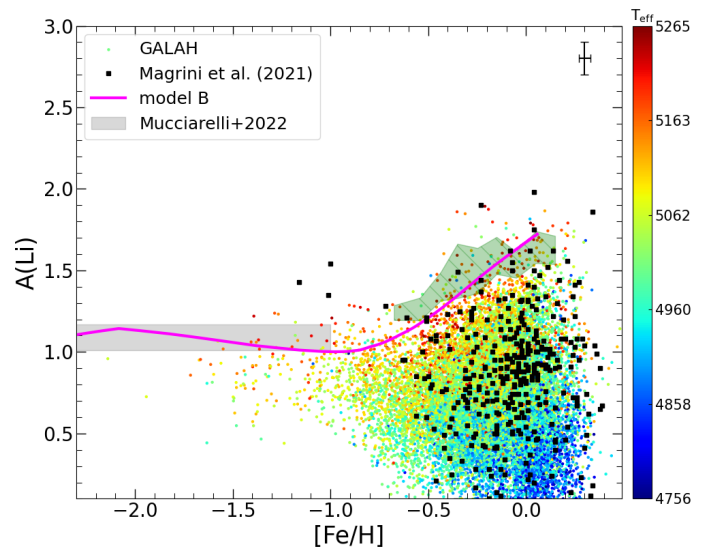


Fig. 10. Li-abundance versus metallicity of early RGB stars from the GALAH and Gaia-ESO catalogues, superimposed with our models (in solid lines). The grey-shaded area is the early RGB plateau from Mucciarelli et al. (2022) ($A(\text{Li}) = 1.09 \pm 0.08$). The black error bars indicate the mean uncertainties from GALAH's sample.

In other words, our chemical evolution model with stellar evolution correction for dwarf-MS and early RGB achieves significant agreement with observations. In particular, in the metal-poor region, by taking into account the ^7Li depletion from stellar models, our chemical evolution model (model B) reproduces very well the Spite plateau, $A(\text{Li}) \sim 2.2$ dex. At the same time, it also reproduces very well the plateau found by Mucciarelli et al. (2022) for early RGB stars, with the averaged $A(\text{Li}) \sim 1.1$ dex. In the high metallicity region, where the nova explosions sensibly contribute to the production of ^7Li , our model B with $^{Li}Y_{\text{Nova}} = 2.34 \times 10^{-5} M_{\odot}$ provides the best fit to the $A(\text{Li})$ data for both early RGB and dwarf-MS stars.

We also include the early RGB stars from the Magrini et al. (2021) catalogue in Fig. 10. In the low metallicity region, no $A(\text{Li})$ plateau is found in their data. This can be understood by the limit on $[\text{Fe}/\text{H}] > -1$ dex of their catalogue. At higher metallicities, our model with stellar ^7Li depletion provides a satisfactory fit to the data.

Finally, we should emphasise that this analysis of the early RGB stars is, in fact, the first attempt we made to study the behaviour of lithium due to the 1DU and previous mixing processes. We relied on the defined upper envelope to draw our findings, as usually done in the literature (Rebolo et al. 1988; Romano et al. 1999; Cescutti & Molaro 2019; Matteucci 2021). However, the presence of Li-rich stars at this evolutionary stage can be problematic for a precise definition of the upper limit (see Casey et al. 2016; Martell et al. 2021, and references therein).

6. Conclusions

We presented in this paper the chemical evolution models for ^7Li of the thin disc of the Milky Way. We adopted data from GALAH DR4 (Wang et al. 2024), the Gaia-ESO surveys (Magrini et al. 2021; Romano et al. 2021), and the sample of Bensby & Lind (2018) for our comparison purpose.

We paid particular attention to two phases of stellar evolution, dwarf-MS and early RGB. The data shows the existence of $A(\text{Li})$ plateaus, which are the renowned Spite plateau of the

dwarf-MS stars and the early RGB plateau. The second plateau was recently discovered by Mucciarelli et al. (2022) and is also seen in our sample.

The depletion of ^7Li abundance from the primordial value ($A(\text{Li}) = 2.69$ dex) during the PMS evolution of low-mass metal-poor stars due to the efficiency of envelope overshooting was recently studied in Nguyen et al. (2025). We investigated the amount of depletion at these two evolutionary stages, MS and early RGB (when the 1DU is already completed), from their stellar models. In this work, our chemical evolution models assumed the gas compositions have the primordial lithium ($A(\text{Li}) = 2.69$ dex) and evolved further with the contributions from nova explosions from binary systems. Together with the corrections from stellar models, we found the chemical evolution model with the total produced ^7Li yield during a nova's lifetime $^{Li}Y_{\text{Nova}} = 2.34 \times 10^{-5} M_{\odot}$ to provide the best-fit model for the galactic lithium in the thin disc. The model consistently reproduced the ^7Li abundances of both the dwarf-MS and the early RGB samples. These results lend support to the depletion suggested from the modification models of Nguyen et al. (2025) if we assume to have primordial gas with a cosmological abundance of lithium, and constrain the amount of lithium yield that is produced by nova systems. In this regard, it should be noted that we assumed all novae produce the same amount of ^7Li during their lifetimes. A more complex model with the dependency of $^{Li}Y_{\text{Nova}}$ on stellar mass, metallicity or delay timescale might help us to have more precise constraints.

Besides that, for the sake of completeness, we mention that the only interstellar ^7Li measurement in metal-poor material provides a ^7Li abundance in agreement with that of warm halo, suggesting a different solution from the stellar is required to explain the “cosmological lithium problem” (Molaro et al. 2024). In this regard, we should clarify that our attempt in this work by using the correction from stellar models to reproduce the Spite plateau does not rule out the possibility that the interstellar gas composition has the measured dwarf-MS stars ^7Li abundance ($A(\text{Li}) \approx 2.2$ dex). This possibility requires more thorough investigations and will be addressed in the coming work.

Finally, Molaro et al. (2020a) studied the ^7Li abundance in the accreted dwarf galaxy of Gaia-Sausage-Enceladus, Monaco et al. (2010) in ω Centauri, Mucciarelli et al. (2014) in the Sagittarius globular cluster M54, and Matteucci et al. (2021) presented chemical evolution models of ^7Li for dwarf spheroidal and ultra-faint galaxies. The authors concluded that the Spite plateau could be a universal feature. This broadens the possibility of testing the internal mixing processes from stellar models, namely, whether they are needed and/or their efficiencies. A comprehensive study on this topic is reserved for future work.

Acknowledgements. The authors are thankful to Paolo Molaro for his insight and thorough suggestions to improve this paper. This project has received funding from the European Union's Horizon 2020 research and innovation programme under grant agreement No 101008324 (ChETEC-INFRA). CTN and FR acknowledge the support by INAF Mini grant 2024, “GALoMS – Galactic Archaeology for Low Mass Stars” (1.05.24.07.02). AJK acknowledges support by the Swedish National Space Agency (SNSA). GE acknowledges the contribution of the Next Generation EU funds within the National Recovery and Resilience Plan (PNRR), Mission 4 - Education and Research, Component 2 - From Research to Business (M4C2), Investment Line 3.1 - Strengthening and creation of Research Infrastructures, Project IR0000034 – “STILES - Strengthening the Italian Leadership in ELT and SKA”. FR is a fellow of the Alexander von Humboldt Foundation. FR acknowledges support by the Klaus Tschira Foundation. FR and GC acknowledge financial support under the National Recovery and Resilience Plan (NRRP), Mission 4, Component 2, Investment 1.1, Call for tender No. 104 published on 2.2.2022 by the Italian Ministry of University and Research (MUR), funded by the European Union - NextGenerationEU - Project ‘Cosmic POT’ (PI: L. Magrini) Grant Assignment Decree No. 2022X4TM3H by the Italian Ministry of Ministry of University and Research (MUR). L.M., and G.C. thank

I.N.A.F. for the 1.05.23.01.09 Large Grant - Beyond metallicity: Exploiting the full Potential of Chemical elements (EPOCH) (ref. Laura Magrini). A.M., and D.R. acknowledge support from the project “LEGO – Reconstructing the building blocks of the Galaxy by chemical tagging” (P.I. A. Mucciarelli), granted by the Italian MUR through contract PRIN 2022LLP8TK_001. Supported by Italian Research Center on High Performance Computing Big Data and Quantum Computing (ICSC), project funded by European Union - NextGenerationEU - and National Recovery and Resilience Plan (NRRP) - Mission 4 Component 2 within the activities of Spoke 3 (Astrophysics and Cosmos Observations).

References

- Arai, A., Tajitsu, A., Kawakita, H., & Shinnaka, Y. 2021, *ApJ*, 916, 44
- Bensby, T., Bergemann, M., Rybizki, J., et al. 2019, *The Messenger*, 175, 35
- Bensby, T. & Lind, K. 2018, *A&A*, 615, A151
- Bonifacio, P. 2002, *A&A*, 395, 515
- Borisov, S., Prantzos, N., & Charbonnel, C. 2024, *A&A*, 691, A142
- Bressan, A., Marigo, P., Girardi, L., et al. 2012, *MNRAS*, 427, 127
- Buder, S., Sharma, S., Kos, J., et al. 2021, *MNRAS*, 506, 150
- Casey, A. R., Ruchti, G., Masseron, T., et al. 2016, *MNRAS*, 461, 3336
- Cescutti, G. & Molaro, P. 2019, *MNRAS*, 482, 4372
- Charbonnel, C. & Primas, F. 2005, *A&A*, 442, 961
- Charbonnel, C. & Zahn, J. P. 2007, *A&A*, 467, L15
- Coc, A., Uzan, J.-P., & Vangioni, E. 2014, *J. Cosmology Astropart. Phys.*, 2014, 050
- Coc, A., Vangioni-Flam, E., Descouvemont, P., Adahchour, A., & Angulo, C. 2004, *ApJ*, 600, 544
- Cybur, R. H., Fields, B. D., & Olive, K. A. 2003, *Physics Letters B*, 567, 227
- Cybur, R. H., Fields, B. D., Olive, K. A., & Yeh, T.-H. 2016, *Reviews of Modern Physics*, 88, 015004
- Dantas, M. L. L., Smiljanic, R., Romano, D., et al. 2025, *arXiv e-prints*, arXiv:2505.17173
- D’Antona, F. & Matteucci, F. 1991, *A&A*, 248, 62
- De Silva, G. M., Freeman, K. C., Bland-Hawthorn, J., et al. 2015, *MNRAS*, 449, 2604
- Della Valle, M. & Izzo, L. 2020, *A&A Rev.*, 28, 3
- Ding, M.-Y., Shi, J.-R., Yan, H.-L., et al. 2024, *ApJS*, 271, 58
- Eggenberger, P., Buldgen, G., Salmon, S. J. A. J., et al. 2022, *Nature Astronomy*, 6, 788
- Eggenberger, P., Haemmerlé, L., Meynet, G., & Maeder, A. 2012, *A&A*, 539, A70
- Ford, H. C. 1978, *ApJ*, 219, 595
- Franciosini, E., Randich, S., de Laverny, P., et al. 2022, *A&A*, 668, A49
- Fu, X., Bressan, A., Molaro, P., & Marigo, P. 2015, *MNRAS*, 452, 3256
- Fu, X., Romano, D., Bragaglia, A., et al. 2018, *A&A*, 610, A38
- Gao, J., Zhu, C., Lü, G., et al. 2024, *ApJ*, 971, 4
- Gao, Q., Shi, J.-R., Yan, H.-L., et al. 2019, *ApJS*, 245, 33
- Gao, X., Lind, K., Amarsi, A. M., et al. 2020, *MNRAS*, 497, L30
- Greggio, L. & Renzini, A. 1983, *A&A*, 118, 217
- Iliadis, C. & Coc, A. 2020, *ApJ*, 901, 127
- Izzo, L., Della Valle, M., Mason, E., et al. 2015, *ApJ*, 808, L14
- Izzo, L., Molaro, P., Bonifacio, P., et al. 2018, *MNRAS*, 478, 1601
- Izzo, L., Siebert, T., Jean, P., et al. 2025, *arXiv e-prints*, arXiv:2504.20866
- Koch, A., Lind, K., Thompson, I. B., & Rich, R. M. 2012, *Memorie della Societa Astronomica Italiana Supplementi*, 22, 79
- Komatsu, E., Smith, K. M., Dunkley, J., et al. 2011, *ApJS*, 192, 18
- Korn, A. J., Grundahl, F., Richard, O., et al. 2007, *ApJ*, 671, 402
- Kroupa, P. 2001, *MNRAS*, 322, 231
- Lind, K., Primas, F., Charbonnel, C., Grundahl, F., & Asplund, M. 2009, *A&A*, 503, 545
- Lodders, K., Palme, H., & Gail, H. P. 2009, *Landolt Börnstein*, 4B, 712
- Magrini, L., Lagarde, N., Charbonnel, C., et al. 2021, *A&A*, 651, A84
- Martell, S. L., Simpson, J. D., Balasubramanian, A. G., et al. 2021, *MNRAS*, 505, 5340
- Matteucci, F. 2021, *A&A Rev.*, 29, 5
- Matteucci, F., D’Antona, F., & Timmes, F. X. 1995, *A&A*, 303, 460
- Matteucci, F. & Greggio, L. 1986, *A&A*, 154, 279
- Matteucci, F., Molero, M., Aguado, D. S., & Romano, D. 2021, *MNRAS*, 505, 200
- Meynet, G. & Maeder, A. 2002, *A&A*, 390, 561
- Molaro, P., Bonifacio, P., Cupani, G., & Howk, J. C. 2024, *A&A*, 690, A38
- Molaro, P., Cescutti, G., & Fu, X. 2020a, *MNRAS*, 496, 2902
- Molaro, P., Izzo, L., Bonifacio, P., et al. 2020b, *MNRAS*, 492, 4975
- Molaro, P., Izzo, L., D’Odorico, V., et al. 2022, *MNRAS*, 509, 3258
- Molaro, P., Izzo, L., Mason, E., Bonifacio, P., & Della Valle, M. 2016, *MNRAS*, 463, L117
- Molaro, P., Izzo, L., Selvelli, P., et al. 2023, *MNRAS*, 518, 2614

- Monaco, L., Bonifacio, P., Sbordone, L., Villanova, S., & Pancino, E. 2010, *A&A*, 519, L3
- Mucciarelli, A., Monaco, L., Bonifacio, P., et al. 2022, *A&A*, 661, A153
- Mucciarelli, A., Salaris, M., Bonifacio, P., Monaco, L., & Villanova, S. 2014, *MNRAS*, 444, 1812
- Nguyen, C. T., Bressan, A., Korn, A. J., et al. 2025, *A&A*, 696, A136
- Nguyen, C. T., Costa, G., Girardi, L., et al. 2022, *A&A*, 665, A126
- Pitrou, C., Coc, A., Uzan, J.-P., & Vangioni, E. 2021, *MNRAS*, 502, 2474
- Planck Collaboration, Ade, P. A. R., Aghanim, N., et al. 2014, *A&A*, 571, A16
- Prantzos, N. 2012, *A&A*, 542, A67
- Randich, S., Pasquini, L., Franciosini, E., et al. 2020, *A&A*, 640, L1
- Rebolo, R., Molaro, P., & Beckman, J. E. 1988, *A&A*, 192, 192
- Richard, O., Michaud, G., & Richer, J. 2005, *ApJ*, 619, 538
- Romano, D., Magrini, L., Randich, S., et al. 2021, *A&A*, 653, A72
- Romano, D., Matteucci, F., Molaro, P., & Bonifacio, P. 1999, *A&A*, 352, 117
- Romano, D., Matteucci, F., Ventura, P., & D'Antona, F. 2001, *A&A*, 374, 646
- Shafter, A. W. 1997, *ApJ*, 487, 226
- Singh, V., Bhowmick, D., & Basu, D. N. 2024, *Astroparticle Physics*, 162, 102995
- Singh, V., Lahiri, J., Bhowmick, D., & Basu, D. N. 2019, *Soviet Journal of Experimental and Theoretical Physics*, 128, 707
- Spite, F. & Spite, M. 1982a, *A&A*, 115, 357
- Spite, M. & Spite, F. 1982b, *Nature*, 297, 483
- Tajitsu, A., Sadakane, K., Naito, H., Arai, A., & Aoki, W. 2015, *Nature*, 518, 381
- Tajitsu, A., Sadakane, K., Naito, H., et al. 2016, *ApJ*, 818, 191
- Travaglio, C., Randich, S., Galli, D., et al. 2001, *ApJ*, 559, 909
- Wang, E. X., Nordlander, T., Buder, S., et al. 2024, *MNRAS*, 528, 5394